remote sensing

MDPI

Article

Delineation of Wetland Areas in South Norway from Sentinel-2 Imagery and LiDAR Using TensorFlow, U-Net, and Google Earth Engine

Vegar Bakkestuen [1,*], Zander Venter [1], Alexandra Jarna Ganerød [2,3] and Erik Framstad [1]

[1] Norwegian Institute for Nature Research, Sognsveien, 0855 Oslo, Norway
[2] Department of Geography, Norwegian University of Science and Technology, 7049 Trondheim, Norway
[3] Geological Survey of Norway (NGU), 7040 Trondheim, Norway
* Correspondence: vegar.bakkestuen@nina.no

Abstract: Wetlands are important habitats for biodiversity and provide ecosystem services such as climate mitigation and carbon storage. The current wetland mapping techniques in Norway are tedious and costly, and remote sensing provides an opportunity for large-scale mapping and ecosystem accounting. We aimed to implement a deep learning approach to mapping wetlands with Sentinel-2 and LiDAR data over southern Norway. Our U-Net model, implemented through Google Earth Engine and TensorFlow, produced a wetland map with a balanced accuracy rate of 90.9% when validated against an independent ground-truth sample. This represents an improvement upon manually digitized land cover maps in Norway, which achieved accuracy rates of 46.8% (1:50,000 map) and 42.4% (1:5000 map). Using our map, we estimated a total wetland coverage area of 12.7% in southern Norway, which is double the previous benchmark estimates (5.6%). We followed an iterative model training and evaluation approach, which revealed that increasing the quantity and coverage of labeled wetlands greatly increases the model performance. We highlight the potential of satellite-based wetland maps for the ecosystem accounting of changes in wetland extents over time—something that is not feasible with traditional mapping methods.

Keywords: remote sensing; neural network; deep learning; land cover; wetland; machine learning

Citation: Bakkestuen, V.; Venter, Z.; Jarna Ganerød, A.; Framstad, E. Delineation of Wetland Areas in South Norway from Sentinel-2 Imagery and LiDAR Using TensorFlow, U-Net, and Google Earth Engine. *Remote Sens.* **2023**, *15*, 1203. https://doi.org/10.3390/rs15051203

Academic Editor: Isam Shahrour

Received: 22 January 2023
Revised: 17 February 2023
Accepted: 18 February 2023
Published: 22 February 2023

1. Introduction

Wetlands are ecosystems that are permanently or periodically saturated or inundated with water and include habitats in the transition between terrestrial and freshwater or marine ecosystems. They offer a wide range of ecosystem services, including water purification, flood control and carbon sequestration [1,2]. Wetlands hold the highest density of soil carbon among terrestrial ecosystem types [3]. This makes them efficient and cost-effective nature-based solutions to climate change, as they sequester atmospheric carbon and are important in the long-term storage of carbon [4]. Despite this, wetlands are constantly under pressure from human activities [5,6,7], and wetland habitat losses due to land-use change often lead to decreases in local biodiversity and altered hydrological cycles, which result in carbon emissions.

It has been estimated that about 9% of the mainland of Norway is covered by open wetlands [8]. Open peatlands, which include open bogs and fens, are the wetland types with the highest coverage rate in Norway (approximately 8% of land cover; [8]. However, the coverage of wetlands over Norway remains uncertain, as different data sources yield different estimates (e.g., 3.8% in 1:5000 maps [9] vs. 6.0% in 1:50,000 [10]and vs. 5.3% in official statistics [11]. This is partly because previous mapping efforts have been based on manual in situ mapping procedures, which require substantial financial investment and adopt differing definitions of wetland habitats. There are, however, several concerns

regarding these map layers, including: (1) the landcover classification system suitable for topographic mapping at a scale of 1:50,000 is coarse; (2) small polygons are kept or removed selectively for cartographic reasons; (3) the main method for the 1:50,000 layer is aerial photo interpretation without field validation; and (4) the 1:5000 layer is not mapped in mountainous areas, where many wetlands are excluded from national estimates [8]. Furthermore, employing fieldworkers to digitize habitat types introduces a sampler bias, which makes the resulting map vulnerable to spatial and temporal inconsistencies [12,13,14,15] Mapping instructions and methods can also change over time, making it difficult to discern whether changes in wetland cover are real or merely an artifact of changes in mapping methodology. Apart from the mostly single-timepoint aerial coverage estimates, there is little active monitoring and surveillance of wetland conditions or changes over time. However, the active monitoring and annual or biennial mapping of wetlands will become important given the revised management plan for the restoration of wetlands in 2021 [16].

Due to the importance of wetlands for ecosystem services, and the threats of anthropogenic disturbance, monitoring and mapping wetlands is important to aid in their conservation. The remote sensing of wetlands has seen increased attention in recent years, with many large-scale studies illustrating the ability to map wetlands from satellite images using machine learning techniques [17,18]. The current wetland mapping techniques in Norway are tedious and costly, but satellite and airborne remote sensing methods including optical sensing, radar sensors, and LiDAR provide an opportunity for large-scale mapping and ecosystem accounting. So far, Norway has not supplemented in situ wetland inventories and mapping with remote sensing data and machine learning classification workflows, which stands in contrast to countries such as Canada [19]. Perhaps the most important thing to note is that Norway until recently has lacked access to high-quality ground truths, which are necessary for training, calibrating, and validating satellite-based wetland maps [20].

Few studies have applied deep learning models to wetland classification [17], and to the best of our knowledge only [21] has done so using a fusion of Sentinel-1 and Sentinel-2 data. In a meta-analysis of more than 200 publications, [22] found that the median accuracy for classifying land use and land cover using deep learning models was 91%, and that there was no other tree- or kernel-based classifier that achieved a median accuracy over 90%. Therefore, although less sophisticated models are more efficient in terms of the training data requirement and inference speeds, deep learning models ultimately achieve higher accuracies for land cover classification.

In the literature review by [18], which also included the data base from [17], we found very few examples on the deep learning classification of wetlands by use of Sentinel-1 or -2. One exemption was [21], who used deep learning for land use and land cover (LULC) classification based on U-Net based on Sentinel-1 and -2. Another exemption was also [23], who used deep U-Net convolutional networks and Sentinel-2 imagery for coastal wetland classification. By comparing deep learning and shallow learning for large-scale wetland classification in Alberta, Canada, [24] found that the accuracy of the convoluted neural networks (CNN) product was about 80%. [24] also concluded that CNNs may be better able to capture natural complexities within wetland classes. In this study, we explored the potential of using deep learning to map wetlands at a regional scale using U-Net convolutional networks and cloud computation on Sentinel-2 and LiDAR data.

To distinguish wetlands from other land use and land cover types (LULC), another type of deep learning method called semantic segmentation is needed. In the process of semantic segmentation, the purpose is to delineate areas with the desired content, in our approach wetlands, from all other unwanted information (i.e., the other LULC classes). This type of deep learning with semantic segmentation often requires the manual digitization of wetlands as polygons, preferably as a wall-to-wall approach in limited areas where training and validation image patches can be cut out and made available for a deep learning training process.

Deep learning has recently been proposed as one of the most promising methods for classifying LULC classes from remote sensed imagery [25]. It has been argued that deep learning can also solve more difficult classification issues such as wetland delineation [26]. Despite the potential for deep learning models, the most common machine learning framework used to generate wetland maps has been decision trees (e.g., Random Forest), followed by support vector machines (SVM) [17]. However, the type of machine learning model adopted has so far had no discernible effect on map accuracy [18].

To meet the demand for wall-to-wall, frequently updatable wetland maps in southern Norway, and to further the international state of wetland remote sensing, our aim was to generate a deep learning-based map of wetlands in Norway using Sentinel-2 imagery and LiDAR data. The integration between Google Earth Engine (GEE) [27] and TensorFlow in the cloud made it possible to apply and train a U-Net model on Sentinel-2 imagery and LiDAR. In this paper, we describe a pipeline on how to classify a land cover type (wetland) using Google Colab [28], TensorFlow, and GEE. Further, we discuss the accuracy and potential of this approach related to other methods.

2. Methods

2.1. Study Area

The study area included the mainland of southern Norway, from 58 to 63°N and from 5 to 13°E, from sea level to 2469 m (Figure 1). It spanned a wide range of environmental gradients relevant to wetland biogeography, including temperature and precipitation regime, solar radiation, geology, and topography gradients [29,30].

Norway is located on the western border of the Baltic Shield, dominated by Precambrian rocks and the Caledonian Mountains with sedimentary, metamorphic bedrock [31]. In July, the average temperatures vary from 17 °C around the Oslo Fjord to 0 °C in the highest peaks of the Jotunheimen Mountain area (Norwegian Meteorological Institute 2023). The monthly average temperatures for January range from −15 °C in Jotunheimen to +3 °C in the outer coastal areas in the south and west. The outer and central areas on the west coast receive the most precipitation, with more than 2000 mm in several areas; however, the interior parts east of the central mountain range receive as little as 200 to 400 mm of annual average rainfall.

In Norway, there are estimated to be approximately 20,500 square kilometers of wetland, i.e., about 5.3% of the total land area [11]. Other major land cover types are open land areas, which includes mountains (38%), forests (37%), fresh water (5%), and agricultural land (3%)[32]. The variation in the mire peatland types in Norway is high and unique, even in a global context [29]. The habitat classification system Nature in Norway 2.2.0 [33] (NiN, in English EcoSyst) includes 13 main habitat types for the wetland ecosystem. These are open fen (V1), bog (V3), mire and swamp forest (V2), tidal and alluvial swamp forest (V8), wet snowbed and snowbed spring (V4 and V5), spring (V6), arctic permafrost wetland (V7), semi-natural fen (V9) and semi-natural wet meadow (V10), peat quarry (V11), drained mire (V12), and artificial wetlands (V13) (see details in https://www.artsdatabanken.no/Pages/172028/Vaatmarkssystemer, in Norwegian). In our study, we did not include the mire and swamp forest classes (classes V2 and V8). Open peatlands, which constitute bogs and fens, are the most common wetland types in Norway (accounting for approximately 95% of open wetland cover; [8].

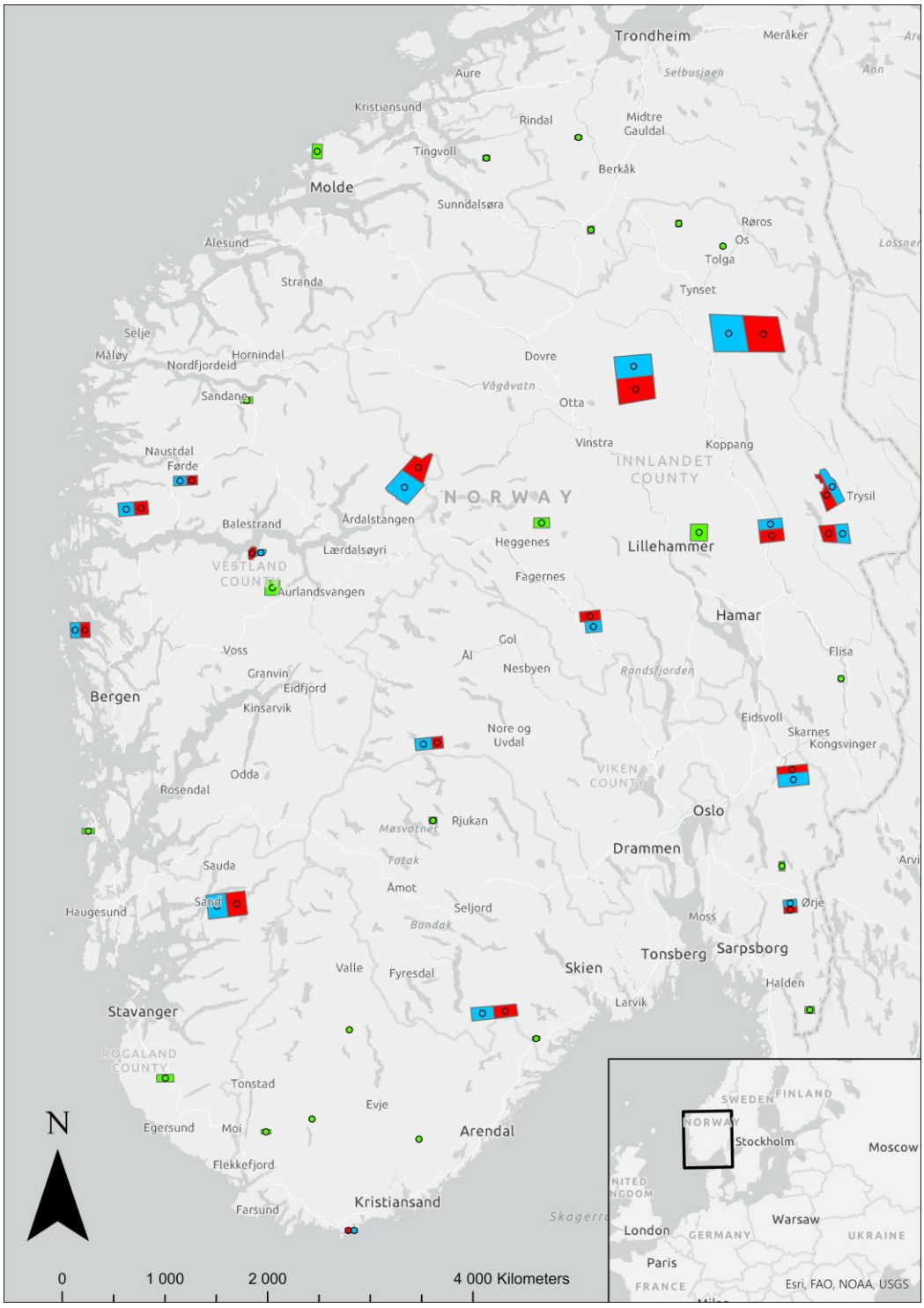

Figure 1. Study area and rectangles for collection of image patches for evaluation (red), original training set (blue), and additional training set (green). The study area is shown in the North-European map in the lower right corner.

In the rectangles shown in Figure 1, there is wall-to-wall digitization of wetland polygons as ground-truth data. Some red and blue rectangles are smaller than others, mainly because they have a higher density and amount of wetland polygons, meaning a lot more effort was needed to map wall-to-wall in these areas. The green rectangles are generally smaller than the red and blue and were created to improve the first deep learning model.

2.2. Preparation of the Predictor Stack

The regional classification of wetlands from Sentinel satellite imagery using deep learning requires access to a large-capacity platform and infrastructure for storing and analyzing large amounts of data. TensorFlow is a software library based on open-source machine learning developed by Google. Pytorch and Keras are examples of other frameworks and libraries. The GEE was used for storing, customizing, and exporting our input data for cloud-based deep learning modeling. Customized files in TensorFlow format (TFRecord-format) were then exported to Google Cloud Storage and used as an input for a virtual machine to process the deep learning scripts in Google Colab.

We processed all Sentinel-2 optical scenes over Norway during August 1 to October 31, 2020. The Sentinel-2 data were used to derive spectrotemporal features as predictor variables [34]. The spectrotemporal features were used to capture both the spectral and temporal (e.g., phenology including autumn color senescence [35,36]) characteristics of land cover classes to offer enhanced model prediction accuracy compared to single-timepoint image classification [37,38].

After trial and error, we selected 3 Sentinel-2 bands and 10 indices, as well as the mean canopy height model from LiDAR (accessed from hoydedata.no) as a substitute for tree height, as our explanatory variables. Using the cloud-masked Sentinel-2 imagery [34], we derived 13 bands or indices (Table 1). For most of these, we used median mosaic values, except for the normalized difference vegetation index (NDVI), where we used the 25th percentile mosaics across the three-month time stack of images.

Table 1. List of input variables from Sentinel-2 in the deep learning model showing the names, abbreviations, equations, and references for equations. See footnotes for the various Sentinel-2 bands that were used.

Number	Name	Abbreviation	Equation	Statistics	Reference
1	The green band 3	B3	b3	Median	
2	The near infrared band 8	B8	b8	Median	
3	The red edge band swir4 band 12	B12	b12	Median	
4	The normalized difference vegetation index	NDVI	((b8 − b4)/(b8 + b4))	The 25th percentile	[39]
5	The normalized burn ratio	NBR	((b8 − b12)/(b8 + b12))	Median	[40]
6	The normalized difference red/green	REDGREEN	((b4 + b3)/(b3 − b4))	Median	
7	The plant senescence reflectance index	PSRI	((b4 − b2)/b6))	Median	[36]
8	The green-red vegetation index	GRVI	((b3 − b4)/(b3 + b4))	Median	[41]
9	The red-edge ratio vegetation index	RERVI	b5/b8	Median	[42]
10	The enhanced vegetation index	EVI	(2.5 * ((b8 − b4)/(b8 + 6 * b4 − 7.5 * b2 + 1))	Median	[43]
11	The carotenoid reflectance index 1	CRI1	((1/b2) − (1/b3))	Median	[44]
12	The green normalized	GNDVI	((b8 -b3)/(b8 + 3))	Median	[45]

13	difference vegetation index The pigment specific simple ratio	PSSR	b8/b4	Median	[46]

* Sentinel-2 bands used: b2 blue (490nm), b3 green (560nm), b4 red (665nm), b5 near infrared 1 (705nm), b6 near infrared 2 (740nm), b8 near infrared 4 (783nm), b12 short wave near infrared 4 (2190nm).

In Norway, LiDAR data are possible to download free of cost from hoydedata.no (accessed 23.04.2022). Both terrain and surface models from LiDAR data were uploaded to GEE. The terrain data can be found on asset "users/vegar/dtm1/dtmcoll", while the surface model can be found on asset "users/vegar/dom1/domcoll". The items can be visualized using this link: 6b56518b215b373147969757a695b4b6—Earth Engine Code Editor (google.com). The index we used was the surface model subtracted by terrain. This index indicates forests, buildings, and other objects that protrude above the terrain. The hypothesis is that open wetlands do not have high index values here.

2.3. Preparation of the Training Data

As a learning basis for the model, wetland polygons had to be annotated or digitized throughout the study area to create image chips or patches that could be used in the deep learning process. The advantage and big difference from using training points as a learning basis, for example, is that deep learning uses large pixel neighborhoods to decide whether a given pixel is a wetland area or something else. In theory, a pixel with some spectral deviation on a huge wetland surface will end up in the wetland class and not create the salt and pepper classification output that is often seen in other classification algorithms.

To avoid creating many thousands of image patches manually, all wetland polygons were digitized wall-to-wall within delimited rectangles. We initially made 17 rectangles over the total study area in southern Norway (see Figure 1). These rectangles were selected based on previous knowledge and field work experience in these areas and to cover a cross-section of different wetland types and regional geographical and climate gradients. As a starting basis for digitizing the wetlands, two sets of orthophotos and existing wetland polygons from the 1:50,000 and 1:5000 map series were used. All polygons and parts of polygons that contained forest were removed either by mapping these via intensive fieldwork or by checking them against new orthophotos or LiDAR data in GIS. Previously unmapped wetland polygons were added to the map, either via intensive field work, via digitization in GIS from orthophotos, or preferably both. The levels of generalization both within and between the existing map bases varied from area to area. The 1:5000 maps also do not have coverage in the mountains. In addition, these maps have different refresh rates. Because of this, a great deal of work was required to create a harmonized data basis for models.

The 17 rectangles varied in size from approximately 25 km^2 to 600 km^2. They were divided into two, so that there were 17 squares that could be used for training purposes and 17 for evaluation. Based on these rectangles, image patches were systematically created through an algorithm made using Google Earth Engine Team (TensorFlow example workflows, Google Earth Engine, Google Developers, last accessed 24 April 2022) measuring 1280 × 1280 m (128 × 128 pixels for our 10-m resolution predictor stack, where the 20-m resolution bands in Sentinel-2 were resampled to 10 m), consisting of the 14 layers from satellite and LIDAR data as well as a rasterized version of the digitized wetlands as a training and evaluation base.

We generated 2000 samples (image patches/chips) for every training and evaluation polygon. All image patches contained one layer with the feature to be predicted or segmented (i.e., wetland) stacked upon all the other layers in the predictor stack (i.e., the 14-layer stack). The image patches from each polygon were merged into a single export

and stored in Google Cloud Storage as a TFRecord. The TFRecord file contains patches of pixel values in each record.

2.4. Computing

GEE was used for storing, customizing, analyzing, and exporting and importing data for cloud-based deep learning modeling. Customized files in TensorFlow format (TFRecord-format) were exported to Google Cloud Storage and used as inputs for the virtual machine to process the deep learning scripts. The model used was a fully convolutional neural network (FCNN) for semantic classification. The goal of semantic segmentation is to label each pixel with a probability estimate of the input image with the class that represents a specific object [47,48].

We used the Keras implementation of the U-Net model [49]. The U-Net model takes 128 × 128-pixel patches as inputs and outputs the per-pixel class probability. The U-Net model is based on the architecture of a TensorFlow workflow made by the Google Earth Engine Team and can be inspected online (TensorFlow example workflows, Google Earth Engine, Google Developers). We used 0.1 as the learning rate, with a batch size of 16, 50 epochs, and 500 steps per epoch. U-Net consists of five encoder and five decoder convolutional layers, each consisting of 32, 64, 128, 256, and 512 channels, plus one center layer with 1024 filters.

For the model settings, for the training gain and evaluation accuracy metrics, we used the 'Adam' as the optimizer, 'Intersection-Over-Union as the loss, and the 'mean Intersection-Over-Union' metric for the accuracy evaluation. The latter meant that 17 samples from the training dataset were used to estimate the error gradient before the model weights were updated. The model was trained with 50 epochs to reach stable output performance. The trained model was then applied to the whole study area by exporting the predictor layers from this area to the cloud storage, where the calculations were performed.

The first U-Net deep learning model performed better near the training and evaluation rectangles than in areas far from these. Therefore, we ran an overlay analysis between our model and existing wetland maps from 1:5000 and 1:50,000 to find areas with major discrepancies. The main discrepancies could be "bad performance" from the deep learning model or that the 1:5000 or 1:50,000 map bases were poorly updated. We found 23 areas where we wanted to improve the model and made an extra set of training rectangles and a similar wall-to-wall map of these (see Figure 1). The size of these additional rectangles was significantly smaller than the original 17 rectangles, and only the conformities were checked and corrected. This process was much faster than the first. The whole workflow is shown in Figure 2.

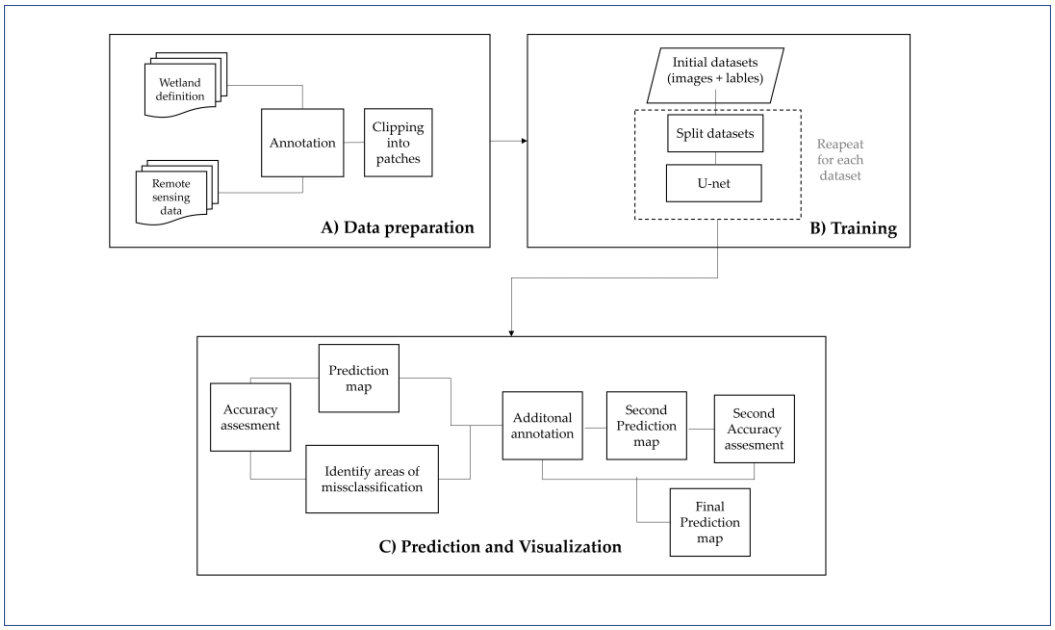

Figure 2. Workflow of the process of predicting open wetlands from Sentinel-2 imagery using TensorFlow and U-Net.

2.5. Unseen Validation Dataset

The wetland model was evaluated with independent ground truths from the national monitoring project ANO (area representative for monitoring in Norway). The ANO consists of 1000 randomly selected 500 × 500 m squares across mainland Norway (Figure 3). The 500 × 500 m squares were randomly drawn from a regular grid across Norway, and the only criterion was that they should not share a common line or corner point. Each ANO square contains 18 circles measuring 250 m² (radius 8.21 m), which are systematically located within the 500 × 500 m square (Figure 3). In the center of each circle, a 1 × 1 m vegetation plot was analyzed, where among other things the coverage of all vascular plants was recorded with the percentage coverage rates.

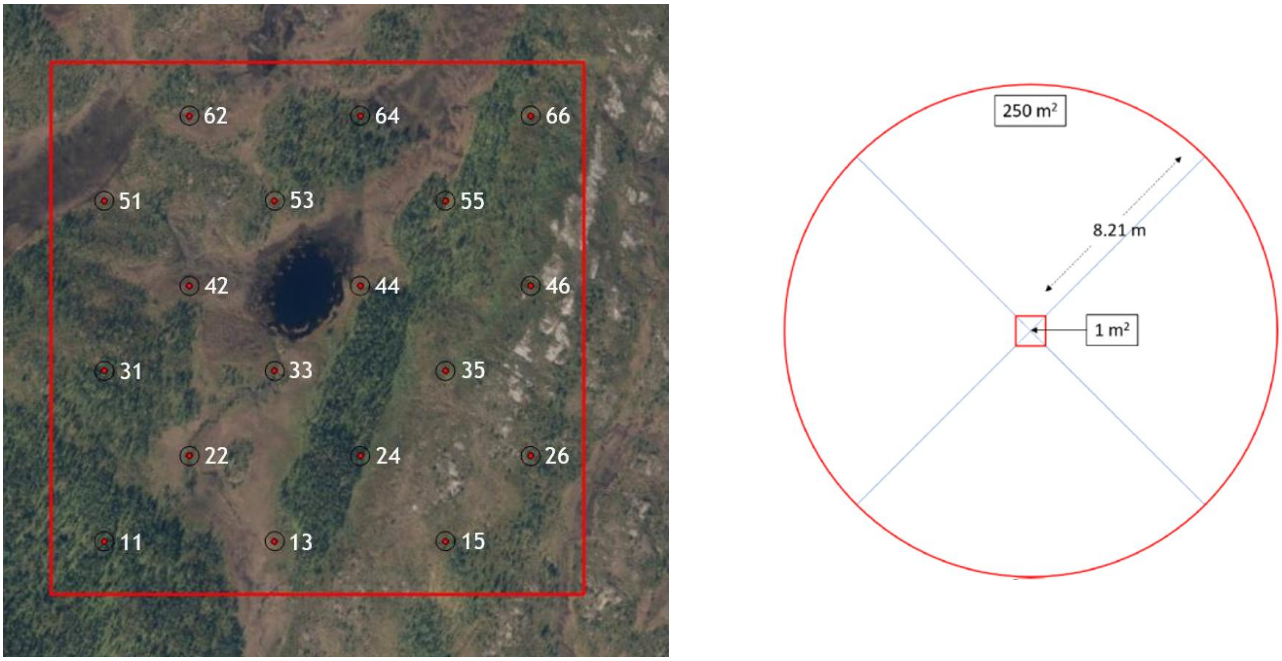

Figure 3. Field design of the unseen validation dataset named as the area representative for monitoring in Norway (ANO), first established in 2019. To the left is an example of a 500 × 500 m

square that contains 18 monitoring circles in a systematically positioned geographical system. To the right is an example of a 250 m^2 monitoring circle with a vegetation sample plot of 1 m^2 in the middle. The main dominating LULC class (percent cover) is allocated to the circle in the field, while both the main LULC class and species estimates are given to the 1 m^2 plot.

In both the 250 m^2 circles and in the 1 m^2 squares, dominant nature types are registered according to the Nature in Norway (NiN) system developed by [33] Halvorsen et al. (2020). Wetlands are divided into 13 different classes according to NiN, where the criterium is mostly related to the species composition. Our wetland model includes all of these NiN wetland classes, except the mire and swamp forest classes (classes V2 and V8).

For the NiN classes that include wetland edges, we accepted an uncertainty margin of one Sentinel-2 pixel (10 m) for a correct hit on a wetland edge. This was done by considering that Sentinel-2 is georeferenced with an inaccuracy rate corresponding to 90% of the pixels having an inaccuracy rate of less than 10 m [50].

A total of 4966 ANO ground truths were available in our study area at both the 250 m^2 scale level and the associated 1 m^2 vegetation plot level at the midpoint of the circle. In the circles at the 250 m^2 level, only the dominant nature type is specified, along with what percentage of the circle this nature type covers. At the 1 m^2 level, the dominant habitat type is also indicated but without a percentage indication, even if several nature types are present. Note that nature types at the 250 m^2 level and 1 m^2 level may be different from each other, although they represent parts of the same area. As conditions for a valid wetland ground truth, we used as criteria that a wetland must cover more than 50% at the 250 m^2 level and that it must either be classified as a wetland at the 1m^2 level or that *Sphagnum* mosses have been registered in the vegetation plot.

3. Results

The first TensorFlow model, based on the 17 original selected training rectangles, was run over 50 epochs until achieving stable performance as measured by inspecting the training gain and evaluation accuracy metrics. The best model had a training mIOUaccuracy rate of 95.6% and validation accuracy rate of 94.9%.

The model output can be inspected here: https://vegar.users.earthengine.app/view/deeplearningmodel1 (accessed on 19 February 2023).

After the identification of areas of mismatches between the first TensorFlow model and existing reference data, a completely new deep learning model was trained on additional annotated data. This model was based on 36 training areas and 17 evaluation areas (rectangles) (Figure 1) and was trained over 50 epochs for stable performance. The new model had 98.51% accuracy for the training data and 98.41% accuracy for the evaluation data. This model corrected most of the weaknesses of the first deep learning model and was considered a better model.

The results of this model can be inspected here: https://vegar.users.earthengine.app/view/deeplearningmodel2 (accessed on 19 February 2023).

Of the 4966 independent ground truths, 547 of these satisfied our criteria as wetlands (Table 2).

Table 2. Estimated error matrix for the final classification with estimates for the user's accuracy (UA) and producer's accuracy (PA).

		Reference			
		Wetland	**Non-wetland**	**Total**	**UA (%)**
Prediction	Wetland	491	351	842	58.3
	Non-wetland	56	4068	4124	98.6
	Total	547	4419	4966	

PA (%)	89.8	92.1

Here, we accepted an uncertainty rate of up to 10 m for NiN wetland edge types. The sensitivity rate of the model was 491/(491 + 56), equaling 89.8%m, and the specificity rate was 4068/(4068 + 351), equaling 92.1%. The balanced accuracy equation was (sensitivity + specificity)/2, i.e., (89.8 + 92.1)/2, equaling 90.9% accuracy.

The corresponding accuracy rates with independent ANO ground truths for the existing reference data for wetlands in Norway were 36.6% for the 1:5000 map basis and 42.2% for the 1:50,000 map. Note that the 1:5000 map does not cover the whole area of Norway and lacks coverage, especially in mountains. Therefore, after correcting for this unmapped area, the true positive rate was 46.8% for these areas according to the ANO ground truths.

We found 351 false positives out of a potential 4419 for our wetland model, which equated to 7.1% misclassifications of non-wetland ground truths. The most common misclassified nature types were nutrient-poor forest types and open heathlands, which are common neighboring nature types to wetlands and often appear together in different mosaics at different scale levels.

Our model estimated that approximately 12.7% of the land area in southern Norway is covered by wetlands (except mires and swamp forests). This was higher than previous estimates (please see the Introduction). The official Norwegian map on a scale of 1:50,000 contains only 5.6% mire areas for all of Norway.

4. Discussion

Our results indicate that as much as 12.7% of the land surface area in southern Norway is covered by wetlands. This is more than double the area of what is mapped in official maps for LULC in Norway. In another study using a point-based survey,[8] estimated that open wetlands in Norway probably cover 8.9% of the total area. Their study was based on an area frame survey of LULC types in a regular 18 × 18 km network (grid) across Norway, where an area of 0.9 km^2 was mapped at each intersection of the grid. The mapping was, however, mainly based on the interpretation of aerial photographs [8].

In the area representative for monitoring (ANO) program that we used for independent ground truths, 11.7% of the area was considered to be wetlands (mire and swamp forest not included) based on the registrations made in the 250 m^2 circles. When we only considered the registrations made in the center vegetation plot on the circles that are at the 1 m^2 scale level, 13.4% of these were assessed as wetlands.

Moreover, there are clear regional patterns where our model predicts more, but also less, wetland areas than the existing maps (see Figures 4 and 5). Our model predicts more wetlands in the mountains and on the west coast of Norway. This agrees with the findings of [8]. There are also regions in Norway where our model has smaller areas with wetland than the existing maps. This is particularly the case in southeastern Norway (see both Figures 4 and 5). This pattern was also observed by [8]. The cause is probably related to the ditching of bogs in the decades after World War II and a general reduction in wetland areas due to construction and other development close to heavily populated areas. The ditching of bogs has led to the bogs being desiccated, planted with trees, and now overgrown by forests. The official maps, thus, appear to be outdated in these areas.

.

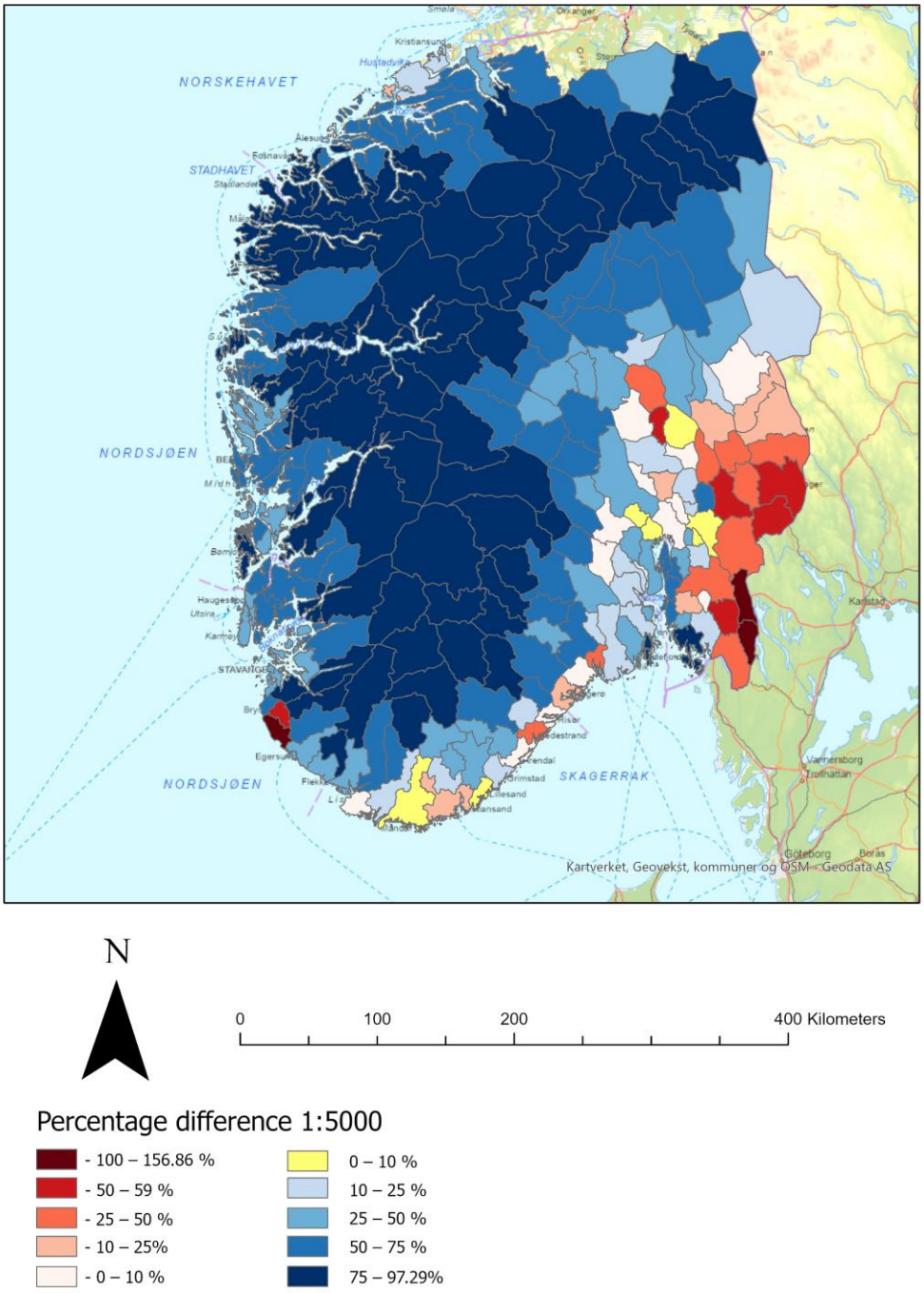

Figure 4. Visualization of the differences in predicted wetland coverage and existing reference data at the scale of 1:5000. Note that the 1:5000 maps do not cover mountain areas, and the large discrepancies in the central part of southern Norway are partly due to this lack of coverage (but see also Figure 5).

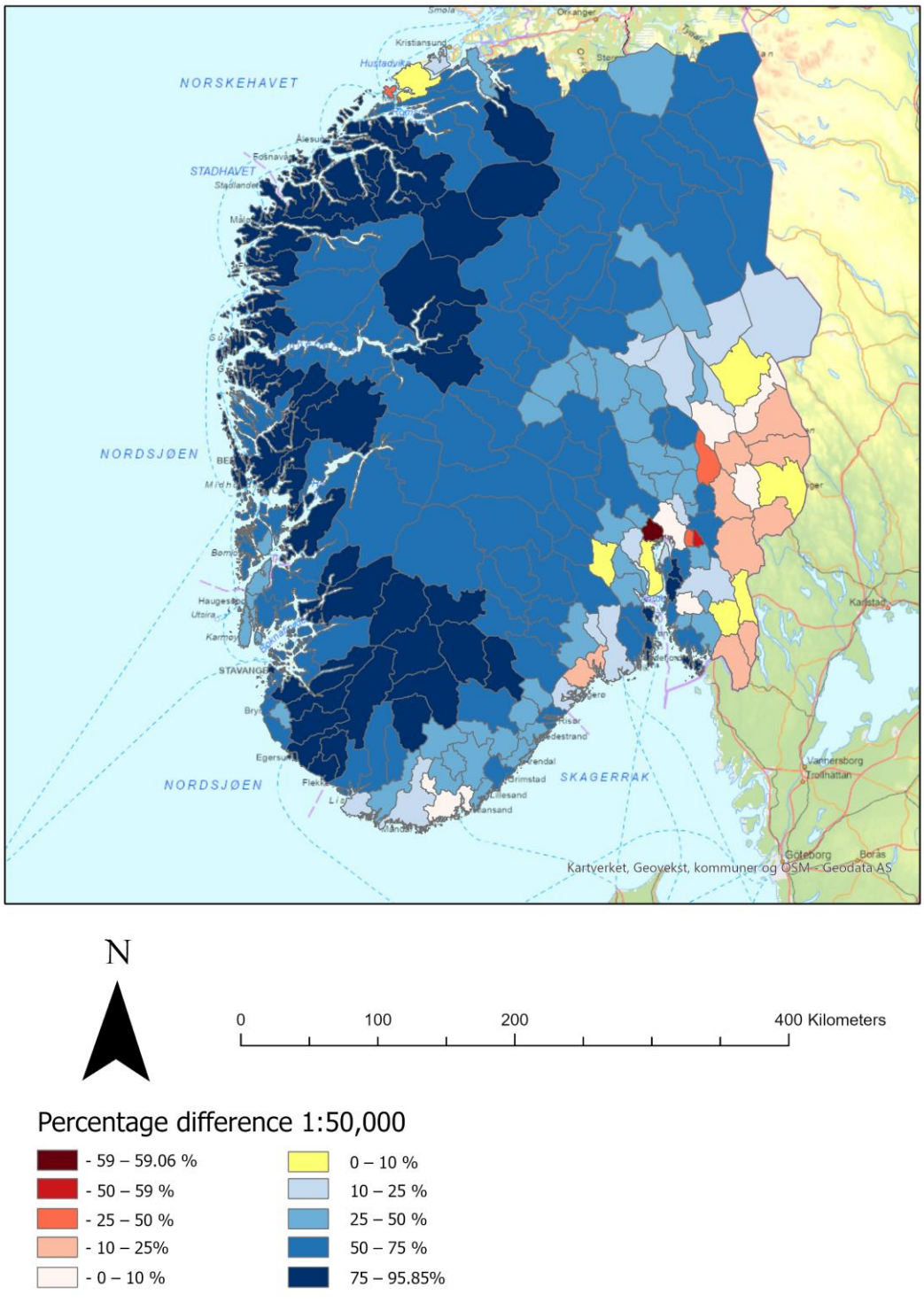

Figure 5. Visualization of the differences in predicted wetland coverage and existing reference data at the scale of 1:50,000.

It was an extensive process and task to create a satisfactory map of wetlands in southern Norway. This was largely due to the lack of satisfactory annotated data, and most of the job involved digitizing wall-to-wall wetland polygons in the rectangles for the collection of image patches. However, the result and the internal deep learning evaluation

accuracy of the final product (98.41%) must be said to be very good compared to earlier studies that aimed to classify wetlands by means of remote sensing. Accuracy rates of 70–95% have been reported in literature studies performed by [26,17,18]. However, only when we introduced an unseen validation dataset for evaluation could a credible confusion matrix be established. We found using this unseen and independent dataset that our model is approximately 90.9% correct for our study area, which is far better than existing reference map data, which is below 50%.

Our model has a balanced accuracy rate of 90.9%, and depending on the further use of the model, users might explore additional filters and post-processing steps to remove some obvious misclassifications and unwanted areas. It will be possible to use the slope to mask out steep areas with a low possibility of being wetlands [51,52]. Additionally, it will be possible to set a threshold on heights above the nearest drainage network. Agricultural land is also annually mapped with a high degree of accuracy in Norway. This agricultural land layer may also be used to mask out misclassified wetlands in these areas.

Initially, a lot of time was spent looking for either spectral bands or indices that formed visual patterns that were in accordance with the wetland delineation we wanted to create. It quickly became clear that single bands or indices alone would not be able to contribute fully to the wetland delineation along the east–west gradient in Norway, nor to different types of wetlands. For instance, indices that seemed to work well in continental areas showed a lower spatial pattern correlation with wetland types in western Norway. It was only when we began to experiment with autumn colors and limited the search for Sentinel-2 images to the period of August–October that the patterns became clearer throughout the study area. The colors yellow, orange, and red, in addition to green, are the most common autumn colors in Norway. The indices that distinguished these colors from each other visually also had the clearest patterns that could distinguish wetlands from other habitat types.

The transfer value of our results is limited by the fact that we did not calculate variable importance scores for the satellite features that informed the deep learning model. Due to funding and time constraints, we were not able to calculate importance scores for the set of predictor variables. We identify this as an avenue for further research given that reducing the feature set can drastically improve the processing and inference times in deep learning architectures [53].

The process of creating the map was iterative, where the first deep learning model based on wetland polygons from 17 rectangles gave good results in the surrounding areas with roughly the same wetland types. However, the models deteriorated when transferred to areas further away from the training rectangles and became quite unreliable 100–200 km from the nearest annotated training area. We, therefore, supplemented the training dataset with new rectangles for wetland types in different regions along altitude, north–south, and east–west (continental) gradients at regular intervals to achieve comparable results with existing maps. This resulted in an updated wetland prediction map of southern Norway that is up to date regarding the input data and now captures new cottage developments and the large-scale ditching of bogs, for which the existing official maps are not yet updated.

It is possible that the use of less training data can give similarly good results by using augmentation methods [54]. We did not try this here, but it may be relevant if the model is to be extended to include northern Norway. However, we felt strongly that the use of a denser network of training rectangles to capture different and other wetland types was important, as the model's performance was significantly poorer with increasing distances from training (and evaluation) rectangles. It is also possible that different models could have been made for specific classes of different types of wetlands and for different regions, such as one model for wetlands in the mountains and one for the lowlands. These are issues that must be tested in future projects to further improve the models. Wetlands must also be said to be a difficult nature type (land cover) to classify [55]. Deep learning methods have also been used to classify other LULC classes with some success [56,57,58]

In recent times, and especially in the last two or three years, an increasing number of papers have been published on the use of U-Net and partly Tensor-Flow in semantic segmentations of imagery. However, these methods are mostly used on very high-resolution images and in remote sensing in products such as WorldView3 and others with a resolution of 1 m or even higher [18]. U-Net has hardly been used on remote sensing products other than RGB and hardly in combinations of Sentinel-1 and Sentinel-2 imagery. One of few exceptions was reported by [21], who used these methods for LULC classification based on U-Net on Sentinel-1 and -2 data. They stated the accuracy to be about 76%, which is quite low. They reported three reasons for this: (1) there were too many details in the classification system; (2) the spatial resolution was too coarse; (3) there were too few observations in the training set (annotations). As we attempted to predict only one LULC class, their first reason did not apply to us. To solve point (reason) 2, we tried to use relevant bands and indices that had as crisp and sharp boundaries between wetlands and other LULC classes as possible. To solve the last point, we invested a lot of time and effort into increasing the amount of annotated data. [21] also stated that the use of a low training basis with annotated data was an important reason for low accuracy in their results. They also stated that they used augmentation to increase the training basis. [59] used BigEarthNet [60] and achieved accuracy rates ranging from 98% (impervious and agricultural areas) to 75% for wetlands. BigEarthNet is a large-scale Sentinel-2 dataset collected from a total of 125 Sentinel-2 tiles covering areas of 10 countries in Europe, with a total of 590,326 tiles measuring 120 × 120 pixels, which are annotated with land cover classification labels.

SAR (Sentinel-1) data were also tested as the input data in our initial phase. However, we ruled out Sentinel-1 bands as predictors as the same wetland (training) polygons often had very different band values in different internal parts. This gave erroneous results, where parts of the wetland polygon were not correctly predicted in the finished classification. U-Net was originally designed to find objects (segments) in very high-resolution images, especially RGB and other low-spectral products [61]. To us, it seems that the method works best on Sentinel imagery when the bands or indices form sharp boundaries and that the polygons' boundaries are in accordance with the boundaries we initially wanted to draw.

5. Conclusions

In our experience, and based on the evidence presented in this paper, the classification of ecosystems and land cover classes based on satellite and repeated airborne remote sensing imagery offers some significant advantages over in situ and manual reference mapping: (1) it covers large areas and multiple years in a consistent and comparable manner, in that it is objectively compared to manual mapping, which is performed by different individuals over different parts of the country; (2) it is scalable to some extent because one can extrapolate over time and space using the deep learning models; (3) it is continually updateable and often available in near real-time, thereby allowing for ongoing monitoring and surveillance (note that LiDAR data are not continuously updated and updates must not rely on this source); (4) it performed better than the existing approaches for reference data validated by regional unseen ground truth data. Whether the kind of deep learning approach presented here or other machine learning methods provide better and more effective classification results must be explored in future studies. A focus on change detection using the methods presented here to account for changes in wetland extents over time would be particularly interesting and critical for effective wetland conservation.

Author Contributions: Conceptualization, V.B.; Methodology, V.B. and A.J.G.; Validation, V.B., Z.V. A.J.G. and E.F.; Formal analysis, V.B.; Writing—original draft, V.B., Z.V. A.J.G. and E.F. Writing— review & editing, V.B, Z.V. A.J.G. and E.F..; Visualization, V.B, and A.J.G. All authors have read and agreed to the published version of the manuscript.

Funding: This research received no external funding.

Data Availability Statement: The results can be viewed at https://vegar.users.earthengine.app/view/deeplearningmodel2 (accessed 14 February 2023).

Conflicts of Interest: The authors declare no conflict of interest.

References

1. Xu, X.; Chen, M.; Yang, G.; Jiang, B.; Zhang, J. Wetland ecosystem services research: A critical review. *Glob. Ecol. Conserv.* 2020, 22, e01027. https://doi.org/10.1016/j.gecco.2020.e01027.
2. Magnussen, K.; Bjerke, J.W.; Brattland, C.; Nybø; S; Vermaat, J. *Verdien av Økosystemtjenester fra Våtmark*; Menon-Publikasjon: Oslo, Norway, 2018. (In Norwegian)
3. Villa, J.A.; Bernal, B. Carbon sequestration in wetlands, from science to practice: An overview of the biogeochemical process, measurement methods, and policy framework. *Ecol. Eng.* **2018**, *114*, 115–128. https://doi.org/10.1016/j.ecoleng.2017.06.037.
4. Taillardat, P.; Thompson, B.S.; Garneau, M.; Trottier, K.; Friess, D.A. Climate change mitigation potential of wetlands and the cost-effectiveness of their restoration. *Interface Focus* **2020**, *10*, 20190129. https://doi.org/10.1098/rsfs.2019.0129.
5. IPBES. *Summary for Policymakers of the Global Assessment Report on Biodiversity and Ecosystem Services*; Intergovernmental Science-Policy Platform on Biodiversity and Ecosystem Services (IPBES): Paris, France, 2019.
6. Sievers, M.; Hale, R.; Parris, K.M.; Swearer, S.E. Impacts of human-induced environmental change in wetlands on aquatic animals. *Biol. Rev.* **2018**, *93*, 529–554. https://doi.org/10.1111/brv.12358.
7. Nybø, S.; Evju, M. Fagsystem for Fastsetting av God Økologisk Tilstand. Forslag fra et Ekspertråd. Ekspertrådet for Økologisk Tilstand, 247 s. 2017. Available online: https://www.regjeringen.no/no/ dokument/rapportar-og-planar/ id438817/ (accessed on 20 February 2023). (In Norwegian with English abstract).
8. Bryn, A.; Strand, G.-H.; Angeloff, M.; Rekdal, Y. Land cover in Norway based on an area frame survey of vegetation types. *Nor. Geogr. Tidsskr.* **2018**, *72*, 131–145.
9. Ahlstrøm, A.P.; Bjørkelo, K.; Fadnes, K. *AR5 Klassifikasjonssystem. Klassifisering av Arealressurser*; NIBIO Bok: 2019; Volume 5. Ås, Norway. (In Norwegian).
10. Norwegian Map Authorities. *Produktspesifikasjon N50 Kartdata: Versjon April 2017*; Statens Kartverk: Hønefoss, Norway, 2017. (In Norwegian)
11. Statistics Norway. *09594: Arealbruk og Arealressurser, Etter Arealklasser (km²) (K) (B) 2011–2022. Statistikkbanken (ssb.no)*; Statistics Norway: Oslo, Norway, 2023.
12. Eriksen, E.L.; Ullerud, H.A.; Halvorsen, R.; Aune, S.; Bratli, H.; Horvath, P.; Volden, I.K.; Wollan, A.K.; Bryn, A. Point of view: Error estimation in field assignment of land-cover types. *Phytocoenologia* **2018**, *49*, 135–148.
13. Ullerud, H.A.; Bryn, A.; Halvorsen, R.; Hemsing, L.Ø. Consistency in land-cover mapping: Influence of field workers, spatial scale and classification system. *Appl. Veg. Sci.* **2018**, *21*, 278–288.
14. Erikstad, L.; Strand, G.-H.; Bentzen, F.; Salberg, A.-B. *Arealrepresentativ Overvåking Basert på Fjernanalyse. Flyfototolkning i Fjell og Myrnatur—NINA Rapport 743*; Norsk Institutt for Naturforskning: Trondheim, Norway, 2011. (In Norwegian with English abstract)
15. Burrough, P.A.; McDonnell, R.A. *Principles of Geographical Information Systems*; Oxford University Press: Oxford, Uk, 1998.
16. Norwegian Environment Agency. *Wetland restoration plan, Norway (2021–2025)*; Report M-1903; 2021
17. Mahdianpari, M.; Granger, J.E.; Mohammadimanesh, F.; Salehi, B.; Brisco, B.; Homayouni, S.; Gill, E.; Huberty, B.; Lang, M. Meta-analysis of wetland classification using remote sensing: A systematic review of a 40-year trend in North America. *Remote Sens.* **2020**, *12*, 1882.
18. Venter, Z.S.; Nowell, M.S.; Bakkestuen, V.; Ruud, A.; Kruse, M.; Skrindo, A.B.; Kyrkjeeide, M.O.; Singsaas, F.T. *Literature Review of Wetland Remote Sensing and Mapping*; NINA Rapport 2014; Norsk Institutt for Naturforskning: Trondheim, Norway, 2021
19. Mahdianpari, M.; Salehi, B.; Mohammadimanesh, F.; Homayouni, S.; Gill, E. The first wetland inventory map of Newfoundland at a spatial resolution of 10 m using sentinel-1 and sentinel-2 data on the google earth engine cloud computing platform. *Remote Sens.* **2019**, *11*, 43.
20. d'Andrimont, R.; Yordanov, M.; Martinez-Sanchez, L.; Eiselt, B.; Palmieri, A.; Dominici, P.; Gallego, J.; Reuter, H.I.; Joebges, C.; Lemoine, G.; et al. Harmonised LUCAS in-situ land cover and use database for field surveys from 2006 to 2018 in the European Union. *Sci. Data* **2020**, *7*, 352. https://doi.org/10.1038/s41597-020-00675-z.
21. Solórzano, J.V.; Mas, J.F.; Gao, Y.; Gallardo-Cruz, J.A. Land Use Land Cover Classification with U-Net: Advantages of Combining Sentinel-1 and Sentinel-2 Imagery. *Remote Sens.* **2021**, *13*, 3600. https://doi.org/10.3390/rs13183600.
22. Ma, L.; Liu, Y.; Zhang, A.; Ye, Y.; Yin, G.; Johnson, B.A. Deep learning in remote sensing applications: A meta-analysis and review. *ISPRS J. Photogramm. Remote Sens.* **2019**, *152*, 166–177. https://doi.org/10.1016/j.isprsjprs.2019.04.015.
23. Dang, K.B.; Nguyen, M.H.; Nguyen, D.A.; Phan, T.T.H.; Giang, T.L.; Pham, H.H.; Nguyen, T.N.; Tran, T.T.V.; Bui, D.T. Coastal Wetland Classification with Deep U-Net Convolutional Networks and Sentinel-2 Imagery: A Case Study at the Tien Yen Estuary of Vietnam. *Remote Sens.* **2020**, *12*, 3270. https://doi.org/10.3390/rs12193270.
24. DeLancey, E.R.; Simms, J.F.; Mahdianpari, M.; Brisco, B.; Mahoney, C.; Kariyeva, J. Comparing Deep Learning and Shallow Learning for Large-Scale Wetland Classification in Alberta, Canada. *Remote Sens.* **2020**, *12*, 2. https://doi.org/10.3390/rs12010002.

25. Yuan, Q.; Shen, H.; Li, T.; Li, Z.; Li, S.; Jiang, Y.; Xu, H.; Tan, W.; Yang, Q.; Wang, J.; et al. Deep learning in environmental remote sensing: Achievements and challenges. *Remote Sens. Environ.* **2020**, *241*, 111716. https://doi.org/10.1016/j.rse.2020.111716
26. Ma, L.; Li, M.; Ma, X.; Cheng, L.; Du, P.; Liu, Y. A review of supervised object-based land-cover image classification. *ISPRS J. Photogramm. Remote Sens.* **2017**, *130*, 277–293. https://doi.org/10.1016/j.isprsjprs.2017.06.001.
27. Gorelick, N.; Hancher, M.; Dixon, M.; Ilyushchenko, S.; Thau, D.; Moore, R. Google Earth Engine: Planetary-scale geospatial analysis for everyone. *Remote Sens. Environ.* **2017**, *202*, 18–27. https://doi.org/10.1016/j.rse.2017.06.031.
28. Bisong, E. Google Colaboratory. In *Building Machine Learning and Deep Learning Models on Google Cloud Platform*; Apress: Berkeley, CA, USA, 2019. https://doi.org/10.1007/978-1-4842-4470-8_7.
29. Moen, A. *National atlas of Norway. Vegetation*; Norwegian Mapping Authority: Hønefoss, Norway, 1999.
30. Bakkestuen, V.; Erikstad, L.; Halvorsen, R. Step-less models for regional environmental variation in Norway. *J. Biogeogr.* **2008**, *35*, 1906–1922. https://doi.org/10.1111/j.1365-2699.2008.01941.x.
31. Sigmond, E.M.O. *Brukerveiledning til Berggrunnskart over Norge. Nasjonalatlas for Norge*; Statens Kartverk: Hønefoss, Norway, 1985. (In Norwegian)
32. Statistics Norway. *Skog, Fjell og Vidde Dominerer-SSB*; Statistics Norway: Oslo, Norway, 2017.
33. Halvorsen, R.; Skarpaas, O.; Bryn, A.; Bratli, H.; Erikstad, L.; Simensen, T.; Lieungh, E. 2020. Towards a systematics of ecodiversity: The EcoSyst framework. Global Ecology and Biogeography. **2020**, *29*, 1887–1906.
34. Venter, Z.S.; Sydenham, M.A.K. Continental-Scale Land Cover Mapping at 10 m Resolution Over Europe (ELC10). *Remote Sens.* **2021**, *13*, 2301. https://doi.org/10.3390/rs13122301.
35. Gómez-Giráldez, P.J.; Pérez-Palazón, M.J.; Polo, M.J.; González-Dugo, M.P. Monitoring Grass Phenology and Hydrological Dynamics of an Oak–Grass Savanna Ecosystem Using Sentinel-2 and Terrestrial Photography. *Remote Sens.*, **2020**, *12*, 600. https://doi.org/10.3390/rs12040600.
36. Merzlyak, M.N.; Gitelson, A.A.; Chivkunova, O.B.; Rakitin, V.Y. Non-Destructive Optical Detection of Pigment Changes during Leaf Senescence and Fruit Ripening. *Physiol. Plant.* **1999**, *106*, 135–141. https://doi.org/10.1034/j.1399-3054.1999.106119.x.
37. Pflugmacher, D.; Rabe, A.; Peters, M.; Hostert, P. Mapping Pan-European Land Cover Using Landsat Spectral-Temporal Metrics and the European LUCAS Survey. *Remote Sens. Environ*. **2019**, *221*, 583–595.
38. Griffiths, P.; Nendel, C.; Pickert, J.; Hostert, P. Towards National-Scale Characterization of Grassland Use Intensity from Integrated Sentinel-2 and Landsat Time Series. *Remote Sens. Environ*. **2019**, *238*, 111124.
39. Tucker, C.J. Red and Photographic Infrared Linear Combinations for Monitoring Vegetation. *Remote Sens. Environ*. **1979**, *8*, 127–150.
40. Snyder, A.; Fulé, P.; Crouse, J. Comparison of burn severity assessment using Differenced Normalized Burn Ratio and ground data. *Int. J. Wildland Fire* **2005**, *14*, 189–198. https://doi.org/10.1071/WF04010.
41. Motohka, T.; Nasahara, K.N.; Oguma, H.; Tsuchida, S. Applicability of Green-Red Vegetation Index for Remote Sensing of Vegetation Phenology. *Remote Sens.* **2010**, *2*, 2369–2387. https://doi.org/10.3390/rs2102369.
42. Cao, Q.; Miao, Y.; Wang, H.; Huang, S.; Cheng, S.; Khosla, R.; Jiang, R. Non-destructive estimation of rice plant nitrogen status with Crop Circle multispectral active canopy sensor. *Field Crops Res.* **2013**, *154*, 133–144. https://doi.org/10.1016/j.fcr.2013.08.005.
43. Huete, A.; Didan, K.; Miura, T.; Rodriguez, E.P.; Gao, X.; Ferreira, L.G. Overview of the radiometric and biophysical performance of the MODIS vegetation indices. *Remote Sens. Environ.* 2002, 83, 195–213. https://doi.org/10.1016/S0034-4257(02)00096-2.
44. Gitelson, A.A.; Zur, Y.; Chivkunova, O.B.; Merzlyak, M.N. Assessing carotenoid content in plant leaves with reflectance spectroscopy. *Photochem. Photobiol.* **2002**, *75*, 272–281. https://doi.org/10.1016/s0034-4257(96)00072-7.
45. Gitelson, A.; Kaufman, Y.J.; Merzlyak, M.N. Use of a green channel in remote sensing of global vegetation from EOS-MODIS. *Remote Sens. Environ.* **1996**, *58*, 289–298.
46. Maleki, M.; Arriga, N.; Barrios, J.M.; Wieneke, S.; Liu, Q.; Peñuelas, J.; Janssens, I.A.; Balzarolo, M. Estimation of Gross Primary Productivity (GPP) Phenology of a Short-Rotation Plantation Using Remotely Sensed Indices Derived from Sentinel-2 Images. *Remote Sens.* **2020**, *12*, 2104. https://doi.org/10.3390/rs12132104.
47. Zhuang, J.; Yang, J.; Gu, L.; Dvornek, N. Shelfnet for fast semantic segmentation. In Proceedings of the 2019 International Conference on Computer Vision Work ICCVW, Seoul, Korea, 27–28 October 2019; pp. 847–56
48. Brown, C.F.; Brumby, S.P.; Guzder-Williams, B.; Birch, T.; Hyde, S.B.; Mazzariello, J.; Czerwinski, W.; Pasquarella, V.J.; Haertel, R.; Ilyushchenko, S.; et al. Dynamic World, Near real-time global 10 m land use land cover mapping. *Sci. Data* **2022**, *9*, 251. https://doi.org/10.1038/s41597-022-01307-4.
49. Chollet, F; et al. Keras. 2015. Available online: https://keras.io. (accessed on 5 January 2023).
50. Stumpf, A.; Michéa, D.; Malet, J.-P. Improved Co-Registration of Sentinel-2 and Landsat-8 Imagery for Earth Surface Motion Measurements. *Remote Sens.* **2018**, *10*, 160. https://doi.org/10.3390/rs10020160.
51. Halabisky, M.; Babcock, C.; Moskal, L.M. Harnessing the Temporal Dimension to Improve Object-Based Image Analysis Classification of Wetlands. *Remote Sens.* **2018**, *10*, 1467. https://doi.org/10.3390/rs10091467.
52. Muro, J.; Varea, A.; Strauch, A.; Guelmami, A.; Fitoka, E.; Thonfeld, F.; Diekkrüger, B.; Waske, B. Multitemporal optical and radar metrics for wetland mapping at national level in Albania. *Heliyon* **2020**, *6*, e04496. https://doi.org/10.1016/j.heliyon.2020.e04496.
53. Wang, J.; Bretz, M.; Dewan, M.A.A.; Delavar, M.A. Machine learning in modelling land-use and land cover-change (LULCC): Current status, challenges and prospects. *Sci. Total Environ.* **2022**, *822*, 153559. https://doi.org/10.1016/j.scitotenv.2022.153559.

54. Shorten, C.; Khoshgoftaar, T.M. A survey on Image Data Augmentation for Deep Learning. *J. Big Data* **2019**, *6*, 60. https://doi.org/10.1186/s40537-019-0197-0.
55. Mahdavi, S.; Salehi, B.; Granger, J.; Amani, M.; Brisco, B.; Huang, W. Remote sensing for wetland classification: A comprehensive review. *GIScience Remote Sens.* **2018**, *55*, 623–658. https://doi.org/10.1080/15481603.2017.1419602.
56. Ball, J.E.; Anderson, D.T.; Chan, C.S. Comprehensive survey of deep learning in remote sensing: Theories, tools, and challenges for the community. *J. Appl. Remote Sens*. **2017**, *11*, 042609.
57. Hoeser, T.; Bachofer, F.; Kuenzer, C. Object Detection and Image Segmentation with Deep Learning on Earth Observation Data: A Review—Part II: Applications. *Remote Sens*. **2020**, *12*, 3053.
58. Kattenborn, T.; Leitloff, J.; Schiefer, F.; Hinz, S. Review on Convolutional Neural Networks (CNN) in Vegetation Remote Sensing. *ISPRS J. Photogramm. Remote Sens*. **2021**, *173*, 24–49.
59. Ulmas, P.; Liiv, I. Segmentation of satellite imagery using U-Net models for land cover classification. *arXiv* **2020**, arXiv:2003.02899.
60. Sumbul, G.; Charfuelan MDemir, B.; Markl, V. Bigearthnet: A large-scale benchmark archive for remote sensing image understanding. In Proceedings of the IEEE International Conference on Geoscience and Remote Sensing Symposium, Yokohama, Japan, 28 July–2 August 2019; pp. 5901–5904. Available online: http: //dx.doi.org/10.1109/IGARSS.2019.8900532 (accessed on 20 February 2023).
61. Ronneberger, O.; Fischer, P.; Brox, T. U-Net: Convolutional Networks for Biomedical Image Segmentation. In *Medical Image Computing and Computer-Assisted Intervention—MICCAI 2015*; Navab, N., Hornegger, J., Wells, W., Frangi, A., Eeds.; MICCAI 2015. Lecture Notes in Computer Science; Springer, Cham, Switzerland, 2015; Volume 9351. https://doi.org/10.1007/978-3-319-24574-4_28.